Title:

An increasing Arctic-Boreal CO_2 sink despite strong regional sources

Coauthors:

Anna-Maria Virkkala[1], Brendan M. Rogers[1], Jennifer D. Watts[1], Kyle A. Arndt[1], Stefano Potter[1], Isabel Wargowsky[1], Edward A. G. Schuur[2,3], Craig See[2], Marguerite Mauritz[4], Julia Boike[5,6], Syndonia M. Bret-Harte[7], Eleanor J. Burke[8], Arden Burrell[1], Namyi Chae[9], Abhishek Chatterjee[10], Frederic Chevallier[11], Torben R. Christensen[12,13], Roisin Commane[14], Han Dolman[15,16], Bo Elberling[17], Craig A. Emmerton[18], Eugenie S. Euskirchen[7], Liang Feng[19], Mathias Goeckede[20], Achim Grelle[21], Manuel Helbig[32,22], David Holl[23], Järvi Järveoja[24], Hideki Kobayashi[25], Lars Kutzbach[23], Junjie Liu[10], Ingrid Liujkx[44], Efrén López-Blanco[12,25], Kyle Lunneberg[26], Ivan Mammarella[27], Maija E. Marushchak[28], Mikhail Mastepanov[12,13], Yojiro Matsuura[29], Trofim Maximov[30], Lutz Merbold[31], Gesa Meyer[32,33], Mats B. Nilsson[24], Yosuke Niwa[34], Walter Oechel[26], Sang-Jong Park[35], Frans-Jan W. Parmentier[36], Matthias Peichl[24], Wouter Peters[44,37], Roman Petrov[30], William Quinton[38], Christian Rödenbeck[20], Torsten Sachs[39], Christopher Schulze[32,40], Oliver Sonnentag[32], Vincent St.Louis[18], Eeva-Stiina Tuittila[41], Masahito Ueyama[42], Andrej Varlagin[43], Donatella Zona[26], and Susan M. Natali[1]

Correspondence: avirkkala@woodwellclimate.org

Affiliations:

1 Woodwell Climate Research Center, Falmouth, USA
2 Center for Ecosystem Science and Society, Northern Arizona University Flagstaff, USA
3 Department of Biological Sciences, Northern Arizona University Flagstaff, USA
4 Biological Sciences, University of Texas at El Paso, El Paso, USA
5 Permafrost Research Section, Alfred Wegener Institute Helmholtz Center for Polar and Marine Research, Potsdam, Germany
6 Department of Geography, Humboldt University, Berlin, Germany
7 Institute of Arctic Biology, University of Alaska Fairbanks, Fairbanks, USA
8 Met Office Hadley Centre, Exeter, UK
9 Institutes of Life Sciences and Natural Resources, Korea University, Seoul, South Korea
10 NASA Jet Propulsion Laboratory, California Institute of Technology, USA
11 Laboratoire des Sciences du Climat et de l'Environnement, LSCE/IPSL, CEA-CNRS-UVSQ, Université Paris-Saclay, Gif-sur-Yvette, France
12 Department of Ecoscience, Arctic Research Center, Aarhus University, Roskilde, Denmark
13 Oulanka research station, University of Oulu, Oulu, Finland
14 Department of Earth and Environmental Sciences, Columbia University, NY, USA
15 Royal Netherlands Institute for Sea Research, Texel, Netherlands
16 Vrije Universiteit, Amsterdam, the Netherlands
17 Department of Geosciences and Natural Resource Management, University of Copenhagen, Copenhagen, Denmark
18 Department of Biological Sciences, University of Alberta, Edmonton, Canada
19 NCEO, School of GeoSciences, University of Edinburgh, UK
20 Max Planck Institute for Biogeochemistry, Jena, Germany
21 Linnaeus University, Växjö, Sweden

22 Department of Physics and Atmospheric Science, Dalhousie University, Halifax, Canada
23 Institute of Soil Science, Center for Earth System Research and Sustainability (CEN), Universität Hamburg, Hamburg, Germany
24 Department of Forest Ecology and Management, Swedish University of Agricultural Sciences, Umeå, Sweden
25 Research Institute for Global Change, Japan Agency for Marine-Earth Science and Technology
26 Department Biology, San Diego State University, San Diego, USA
27 Institute for Atmospheric and Earth System Research / Physics, Faculty of Science, University of Helsinki, Finland
28 Department of Environmental and Biological Sciences, University of Eastern Finland, Finland
29 Forestry and Forest Products Research Institute, Tsukuba, Ibaraki, Japan
30 Institute for Biological Problems of Cryolithozone of the Siberian Branch of the RAS - Division of Federal Research Centre “The Yakut Scientific Centre of the Siberian Branch of the Russian Academy of Sciences”, Yakutsk, Russia
31 Integrative Agroecology, Agroecology and Environment, Agroscope, Zurich, Switzerland
32 Département de géographie, Université de Montréal, Montréal, Québec, Canada
33 Environment and Climate Change Canada, Climate Research Division, Victoria, Canada
34 Earth System Division, National Institute for Environmental Studies /Department of Climate and Geochemistry Research, Meteorological Research Institute, Japan
35 Division of Atmospheric Sciences, Korea Polar Research Institute, Incheon, Republic of Korea
36 Centre for Biogeochemistry in the Anthropocene, Department of Geosciences, University of Oslo, Oslo, Norway
37 Centre for Isotope Research, Energy and Sustainability Research Institute Groningen, Groningen University, The Netherlands
38 Cold Regions Research Centre, Wilfrid Laurier University, Waterloo, Canada
39 GFZ German Research Centre for Geosciences, Germany
40 Department of Renewable Resources, University of Alberta, Edmonton, Canada
41 School of Forest Sciences, University of Eastern Finland
42 Graduate School of Agriculture, Osaka Metropolitan University
43 A.N. Severtsov Institute of Ecology and Evolution, Russian Academy of Sciences, Moscow, Russia
44 Dept. of Meteorology and Air Quality, Wageningen University, The Netherlands

Abstract (151 words)

The Arctic-Boreal Zone (ABZ) is rapidly warming, impacting its large soil carbon stocks. We use a new compilation of terrestrial ecosystem CO_2 fluxes, geospatial datasets and random forest models to show that although the ABZ was an increasing terrestrial CO_2 sink from 2001 to 2020 (mean ± standard deviation in net ecosystem exchange: -548 ± 140 Tg C yr^{-1}; trend: -14 Tg C yr^{-1}, $p<0.001$), more than 30% of the region was a net CO_2 source. Tundra regions may have already started to function on average as CO_2 sources, demonstrating a critical shift in carbon dynamics. After factoring in fire emissions, the increasing ABZ sink was no longer statistically significant (budget: -319 ± 140 Tg C yr^{-1}; trend: -9 Tg C yr^{-1}), with the permafrost region becoming CO_2 neutral (budget: -24 ± 123 Tg C yr^{-1}; trend: -3 Tg C yr^{-1}), underscoring the importance of fire in this region.

Main text (3159 words)

Estimating terrestrial net ecosystem CO_2 exchange (NEE) of the Arctic-Boreal Zone (ABZ) poses a significant challenge[1–4] due to their complex functions [4–6] and a limited network of field measurements [7,8]. As a result, models show a wide range of CO_2 budgets, from substantial net atmospheric sinks (-1,800 Tg C yr^{-1}) to moderate atmospheric sources (600 Tg C yr^{-1}) [1,4,5,9,10], a concerning discrepancy as northern permafrost soils hold nearly half of global soil organic carbon stocks [11]. The release of this soil carbon to the atmosphere as CO_2 could significantly exacerbate climate change [12]. Thus, there is an urgent need to improve CO_2 budget estimates across the ABZ.

The rapid climate change of the ABZ makes this discrepancy even more critical [13]. Increasing air and soil temperatures in both summer and non-summer seasons are causing changes in the CO_2 budget that remain poorly understood [9]. Furthermore, it is not known how the widespread but spatially heterogeneous increase in vegetation productivity and greening [14,15] impacts the annual CO_2 balance although links to enhanced CO_2 sinks during the spring-summer period have been found [16,17]. Some of the enhanced uptake might be offset by CO_2 losses associated with vegetation dieback ('browning'), and the escalating frequency and intensity of disturbances such as abrupt permafrost thaw (e.g., thermokarst), drought and fires, further complicating the understanding of ABZ carbon dynamics and climate feedbacks [18–20].

Current evidence on recent ABZ CO_2 budget trends and their main drivers is limited to few in-situ data-driven synthesis and modeling studies without a regional perspective on where and why CO_2 budgets are changing [1,5,9,10]. These studies have focused primarily on ecosystem CO_2 fluxes (i.e., not incorporating fire emissions), coarse annual or seasonal CO_2 fluxes (i.e., overlooking the intra-annual dynamics), and spatial patterns in CO_2 fluxes with data from only one to two decades. Most importantly, earlier studies have not extended into the 2020s, a period of time where warming has further accelerated and more fires have occurred [21]. Thus, we lack a comprehensive understanding of the regional and seasonal patterns in recent ecosystem CO_2 fluxes, including fire emissions, and their multidecadal trends, and the links to changing environmental conditions across the ABZ.

Here, we address this knowledge gap using the most comprehensive site-level ABZ CO_2 flux dataset to-date —including monthly terrestrial photosynthesis (gross primary production; GPP), ecosystem respiration (R_{eco}), and NEE data from 200 terrestrial eddy covariance and flux chamber sites (4,897 site-months). This dataset is at least four times larger than in earlier upscaling efforts and covers a longer time period with data extending to 2020. The same dataset was previously used to analyze in-situ CO_2 flux trends in permafrost versus non-permafrost regions, with the conclusion that the annual net uptake is increasing in the non-permafrost region but not in the permafrost region [22]. Here we extend that study from the site level to the full ABZ region by combining flux observations with meteorological, remote sensing, and soil data, together with random forest models to estimate CO_2 budgets across the ABZ. We do this upscaling over two periods, 2001-2020 (1-km resolution) and 1990-2016 (8-km resolution); results in the main text are based on the 1-km models unless stated otherwise. We then assess regional and seasonal patterns and trends in ABZ ecosystem CO_2 fluxes and their environmental drivers. We also integrate annual fire emissions from 2002 to 2020 [23] to provide near-complete terrestrial CO_2 budget estimates (referred as NEE + fire).

Results

CO_2 budgets across the ABZ

Using machine learning models that had a high predictive performance (up to two times higher cross-validated R^2 compared to earlier efforts [5,9]), we find that from 2001-2020 circumpolar tundra was on average CO_2 neutral without accounting for fire emissions (in-situ NEE: -4 ± 44 g C m^{-2} yr^{-1}; upscaled NEE: 7 ± 3 g C m^{-2} yr^{-1}; upscaled budget 45 ± 53 Tg C yr^{-1}; mean ± standard deviation; Table 1). In contrast, the boreal was a strong sink (in-situ NEE: -41 ± 82 g C m^{-2} yr^{-1}; upscaled NEE: -43 ± 7 g C m^{-2} yr^{-1}; upscaled budget -593 ± 101 Tg C yr^{-1}). Including fire emissions (on average 237 Tg C yr^{-1} [23], i.e., 2% of R_{eco} and 43% of the ABZ net CO_2 uptake budget) changed the budget to -383 ± 101 Tg C yr^{-1} in the boreal and to 64 ± 53 Tg C yr^{-1} in the tundra. With fire emissions included, the permafrost region turned into CO_2 neutral (NEE: -249 ± 123 Tg C yr^{-1}, NEE + fire: -24 ± 123 Tg C yr^{-1}).

Although the entire ABZ domain was a terrestrial CO_2 sink across all years during 2001-2020 with an average NEE of -548 ± 140 Tg C yr^{-1}, our upscaling of NEE revealed a large areal fraction of annual ecosystem CO_2 sources across the domain (34% of the total region, Fig. 1). For the permafrost domain, the fraction of annual CO_2 sources was even higher (41% of the region). This large fraction is also seen in our in-situ CO_2 flux database, with 30% of sites being CO_2 sources (NEE between 0-142 g C m^{-2} yr^{-1}). These CO_2 source sites were mostly in Alaska (44%), but also in northern Europe (25%), Canada (19%), and Siberia (13%). One key factor driving CO_2 sources is the long and persistent non-summer season (September-May) emissions in the tundra that, on average, exceed the short summer (June-August) net CO_2 uptake (Table 1). In the boreal, longer summers with strong uptake still dominate over non-summer emissions.

Model performance and comparison

We observed moderate correlation of our upscaled NEE results with an ensemble of atmospheric inversions [24] across space (Pearson's correlation 0.5, $p<0.001$), but the correlation between the temporal trends was weaker (Pearson's correlation 0.2, $p<0.001$) (Fig. 1). However, the ensemble net uptake budgets from the inversions, as well as from a global machine-learning based upscaling product (FLUXCOM [25]) were 1.5 to 3 times higher than our upscaled budgets (Supplementary Section 5). Moreover, the global Coupled Model Intercomparison Project Phase 6 (CMIP6) process model ensemble [26] had barely any annual CO_2 sources across the ABZ, indicating that the process models may not accurately simulate CO_2 source situations (Fig. 1), especially given the prevalence of site-level sources. The cross-validated predictive performances of our random forest models for GPP, R_{eco}, and NEE showed high correlations between observed and predicted fluxes (R^2 varied from 0.5 to 0.78 and root mean square error from 19.4 to 37.3 g C m^{-2} $month^{-1}$; Supplementary Fig. 1-3), but upscaling uncertainties remain. For example, areas with the most extensive strong sink or source estimates rarely had in-situ data and were thus largely extrapolated (e.g., sources in central Siberia, or sinks in southern Siberia, Supplementary Fig. 4). These areas also had the highest uncertainties in our analysis (approximately twice as large uncertainties as in the more densely measured areas; Supplementary Fig. 5).

Table 1. Mean gross primary productivity (GPP), ecosystem respiration (R_{eco}), and net ecosystem exchange (NEE) fluxes and budgets over 2001-2020, and NEE + fire budgets from 2002-2020. Uncertainties are standard deviations across sites or pixels (for the mean fluxes) or across bootstrapped budget estimates. Positive numbers for NEE indicate net CO_2 loss to the atmosphere and negative numbers indicate net CO_2 uptake by the ecosystem. Mismatches in the site-level versus upscaled CO_2 fluxes are likely related to sites being biased to certain regions and years while upscaled summaries should provide more representative regional estimates but are influenced by model performance. Mismatches in the NEE vs. GPP-R_{eco} estimates are related to different numbers of sites and observations being available for the different fluxes. Supplementary Table 1 shows the budgets for different vegetation types and regions.

Class	In-situ average			Upscaled per-area average			Average regional budget			The proportion of summer net uptake budget of non-summer net emissions	Average regional budget with fire	Area (x 10^6 km^2)
Flux and unit	NEE g C m^{-2} yr^{-1}	GPP g C m^{-2} yr^{-1}	R_{eco} g C m^{-2} yr^{-1}	NEE g C m^{-2} yr^{-1}	GPP g C m^{-2} yr^{-1}	R_{eco} g C m^{-2} yr^{-1}	NEE Tg C yr^{-1}	GPP Tg C yr^{-1}	R_{eco} Tg C yr^{-1}	%	NEE + fire Tg C yr^{-1}	
Arctic-Boreal Zone	-32 (± 76)	617 (± 396)	587 (± 385)	-26 (± 5)	482 (± 20)	460 (± 15)	-548 (± 140)	9970 (± 144)	9525 (± 90)	1.4	-319	20.79
Tundra	-4 (± 44)	302 (± 124)	311 (± 133)	7 (± 3)	300 (± 14)	306 (± 12)	45 (± 53)	2049 (± 49)	2090 (± 33)	0.9	64	6.8
Boreal	-41 (± 82)	705 (± 402)	664 (± 398)	-43 (± 7)	572 (± 24)	537 (± 17)	-593 (± 101)	7920 (± 106)	7435 (± 74)	1.6	-383	13.9
Permafrost region	-21 (± 62)	459 (± 197)	447 (± 172)	-15 (± 5)	416 (± 20)	405 (± 16)	-249 (± 123)	6918 (± 109)	6719 (± 69)	1.2	-24	16.6

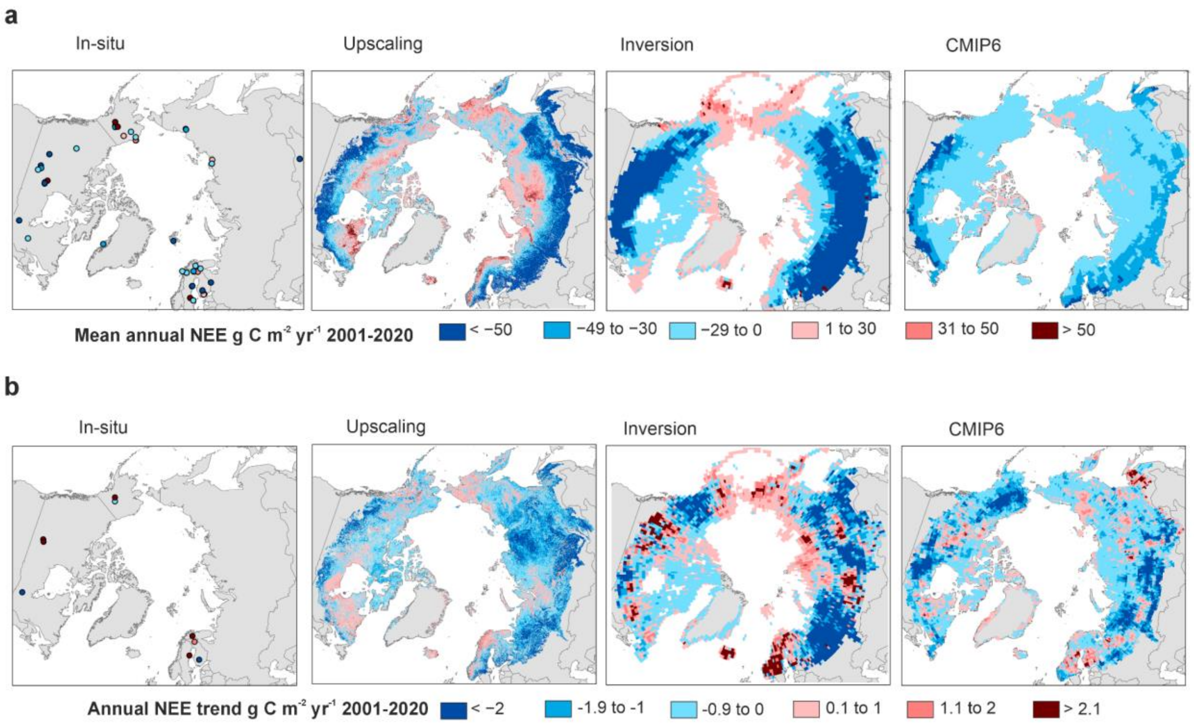

Figure 1. Maps showing the mean annual terrestrial NEE (a) and its trends (b) based on site-level data, our upscaling, atmospheric inversion ensemble, and CMIP6 process model ensemble. In-situ trends in b are based on sites that have >7 years of data. Supplementary Fig. 5c shows the significance of the trends. While the average upscaled NEE values can go up to 116 g C m^{-2} yr^{-1}, most of the values are below 60 g C m^{-2} yr^{-1}. While the NEE values of the inversions can go down to -1636 g C m^{-2} yr^{-1}, most of the values are higher than -200 g C m^{-2} yr^{-1}, similar to upscaling and CMIP6 model outputs.

Temporal trends in upscaled ABZ CO_2 budgets

The ABZ has been an increasing terrestrial CO_2 sink based on NEE alone from 2001 to 2020 (temporal trend: -14 Tg C yr^{-1}, p<0.001) (Fig. 2). However, the increasing sink strength was no longer statistically significant when fire emissions were added to NEE (average NEE + fire budget trend -9 Tg C yr^{-1} over 2002-2020). In the permafrost region, the NEE + fire trend was only 3.3 Tg C yr^{-1}. Nevertheless, based on our NEE upscaling, 23% of the region increased (p<0.05) net CO_2 uptake from 2001 to 2020 (Fig. 1). Most of the increasing net sink activity was driven by an increase in GPP, especially in Siberia (Fig. 2). Some of the trends were also related to a declining R_{eco}, likely associated with disturbed ecosystems (e.g., forest fires, harvesting) with high R_{eco} during the first post-disturbance years now recovering [27]. However, evidence for the increasing overall net uptake trend from the in-situ data is limited due to the low number of long-term sites (>7 years of year-round measurements; 9 sites) out of which only one site showed a statistically significant trend (increasing uptake at a boreal forest site in Finland). Some of the relationships in our model are likely thus influenced by spatial differences across the sites rather than temporal and truly causal patterns, creating some uncertainty in upscaled trends [28]. However, the model reproduces temporal patterns at individual sites well (see Supplementary Fig. 6), and our upscaled trends are similar to a recent in-situ time-series analysis [22] and somewhat similar to those estimated from the inversion ensemble (Fig. 1), providing confidence in our trend results.

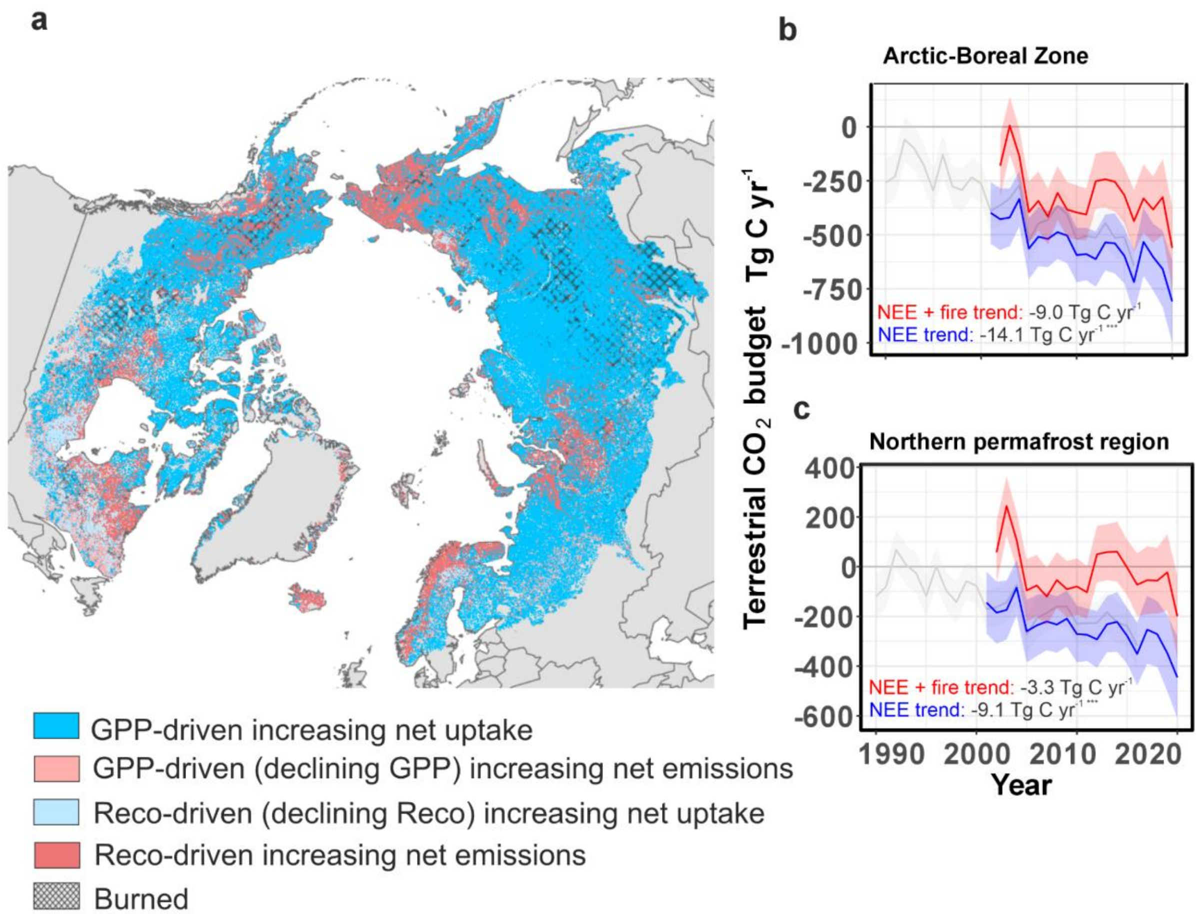

Figure 2. An overlay analysis of NEE, GPP, R_{eco} trend maps identifying how trends in GPP and R_{eco} relate to trends in NEE over 2001-2020 (includes significant and non-significant trends), showing also pixels that burned during 2002-2020 (a). Terrestrial CO_2 budgets for 1-km (blue; 2001-2020) and 8-km (grey; 1990-2016) NEE, and 1-km NEE + fire emissions (red; 2002-2020) across the ABZ (b) and permafrost region (c). Trends are shown for the 2002-2020 (NEE + fire) and 2001-2020 (NEE) periods. Uncertainties are standard deviations in bootstrapped estimates. Stars in the trend values depict the significance of the trend (= p<0.05, **=p<0.01, ***=p<0.001).*

Parts of the ABZ also show increasing annual net CO_2 emissions over time (Fig. 1). Such trends have been observed at six long-term sites (2 to 17 g C m^{-2} yr^{-1}, $p>0.05$), and in 2% of the upscaled region ($p<0.05$) from 2001 to 2020. Most of the increasing net emission trends were driven by an increase in R_{eco} instead of a decline in GPP (Fig. 2). Regions experiencing increased net CO_2 emissions in upscaling were found especially in (i) northern Europe and Canada (dominated by evergreen needleleaf forests with mild and moderately wet climates), (ii) parts of central Alaska and northern Siberia (sparse boreal ecosystems and graminoid tundra with permafrost and high soil carbon stocks), and (iii) Hudson Bay and Siberian lowlands (wetlands with some permafrost and high soil organic carbon stocks). Some sites in Alaska have increasing net emissions of CO_2 due to permafrost thaw [18,29], but it is unclear if similar changes are occurring in other regions with increasing net CO_2 emissions.

We calculated an overall 25% increase in seasonal amplitude of CO_2 fluxes from the upscaled NEE time series from 2001 to 2020 across the ABZ, on par with earlier atmospheric and modeling studies [30,31]. Both increasing summer uptake and non-summer season emissions—the key dynamics driving increasing annual sinks and sources—were evident in the tundra and boreal biomes (Fig. 3). However, over the 2001-2020 period, the increasing uptake (GPP) during summer months dominated over increasing net emissions (R_{eco}) during non-summer months across most of the domain. On average across both biomes, net uptake increased the most during July (an average upscaled increase of -5 g C m^{-2} $month^{-1}$ in the boreal and -3 g C m^{-2} $month^{-1}$ in the tundra in 2011-2020 compared to 2001-2010), and increasing net emissions were occurring throughout the entire non-summer season, with no clear peaks (0.1-0.9 g C m^{-2} $month^{-1}$). Although increases in early growing season (May-June) uptake were evident, late growing season (September) trends were absent or minimal (Fig. 3).

Drivers of ABZ CO_2 fluxes

There are several environmental conditions driving CO_2 budgets across the ABZ. Our variable importance analysis showed CO_2 fluxes, and thus the overall increasing sink strength, are explained by dynamic variables of air or surface temperatures, solar radiation, the Normalized Difference Vegetation Index (NDVI), and partially also by soil temperature, snow cover, and the vapor pressure deficit (Supplementary Fig. 8-10). Other less important dynamic variables were vegetation cover and atmospheric CO_2 concentration. Volumetric soil water content was not important in our models, likely due to the large uncertainties and coarse spatial resolution in the gridded product, although in-situ studies have shown drier soils to be linked to larger net CO_2 emissions and wetter soils to enhanced plant growth due to the lack of water limitation [32]. Static variables (primarily vegetation type, soil carbon stock, soil pH) were also important in explaining spatial differences.

The most important dynamic variables had a positive overall effect on net uptake, GPP, and R_{eco} (Supplementary Fig. 8-10), however, these relationships are more nuanced in reality. In fact, the recent permafrost in-situ trend analysis of CO_2 fluxes using the same database suggests that the CO_2 flux response to warmer temperatures ranges from positive to negative, depending on the availability of water and nutrients at the site [22]. Consequently, strong warming or greening trends did not always translate into increasing net CO_2 sinks in our upscaling (Supplementary Fig. 11). For example, while 49% of the region experienced greening (June-August average NDVI; based on MODIS NDVI, $p<0.05$), only 12% of those greening pixels showed an annual increasing net CO_2 uptake trend, and 29% an increasing June-August net uptake.

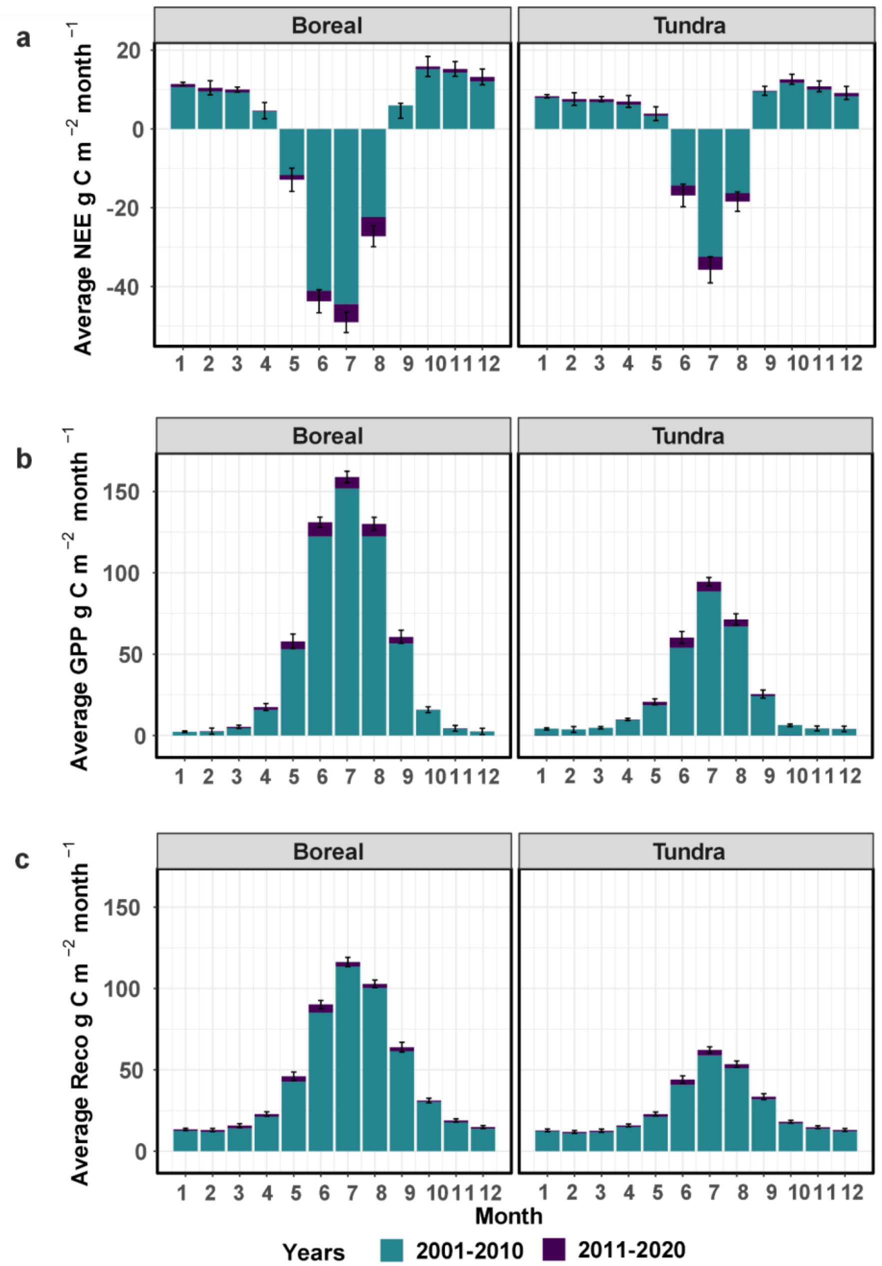

Figure 3. Average upscaled monthly NEE, GPP, and R_{eco} in boreal and tundra biomes during the past two decades. Negative NEE values represent net uptake and positive net release. Error bars represent standard deviations across bootstrapped estimates and are only shown for the 2011-2020 period but are similar for the 2001-2010 period. Note that NEE was 1.4 g C m^{-2} $month^{-1}$ lower in September 2011-2020 compared to 2001-2020 in the boreal biome, but this is not shown in the figure. For a similar figure made based on the in-situ data, see Supplementary Fig. 7.

Continental and regional patterns in CO_2 budgets and their trends

Our upscaling showed clear continental patterns in NEE budgets and trends (Fig. 4), with the boreal biome primarily driving the budget and trend differences between the continents [1,33]. The increasing net uptake trend was more pronounced in Eurasia (-11 Tg C yr^{-1}, $p<0.001$) compared to North America (-3 Tg C yr^{-1}, $p<0.05$), which corresponds with the smaller area, weaker warming, declining snow cover and greening trends in North America (Supplementary Fig. 12-14). We found statistically significant declining summer soil moisture trends in Siberian boreal (Supplementary Fig. 15), but this did not translate into stronger net emissions. When fire emissions were added, continental differences were less pronounced due to the much larger and more rapidly increasing CO_2 emissions from Siberian fires (on average 160 compared to 76 Tg C yr^{-1} in North America; Supplementary Fig. 16). Fire emissions even reversed some NEE trends: the strong increasing sink in Siberia became a source when fire emissions were included (trend: +0.7 Tg C yr^{-1}; $p > 0.05$). However, Siberian ecosystems have the largest uncertainty for both the upscaled fluxes and inversion-based estimates due to lack of in situ observations, making it challenging to accurately determine the magnitude of continental differences (Fig. 4, Supplementary Fig. 17).

Alaska is an important contributor in the weaker North American CO_2 sink. Based on our analysis, Alaska as a whole was consistently CO_2 neutral or a source over 2002-2020 (NEE + fire emissions), both in the boreal (budget +5 Tg C yr^{-1}) and tundra (budget +7 Tg C yr^{-1}). Alaska has a relatively high density of observations, making this result more certain compared to other regions. Alaska is therefore different from the other ABZ regions where boreal regions still remain on average CO_2 sinks. Potential reasons for the Alaskan CO_2 source include Alaska having the most rapidly warming autumns and declining autumn snow cover, which has high inter-annual variability (Supplementary Fig. 14 and 18). Further, field measurements suggest that many of the observed changes in Alaskan ecosystems can be attributed to permafrost thaw [18,29]—a phenomenon that has accelerated significantly in response to Alaska's pronounced warming trend since the 1950s [34]. However, we were unable to incorporate permafrost thaw into our models as high-resolution geospatial data from 1990 to 2020 were not available. The question of whether analogous trends will manifest in other regions across the northern permafrost region remains an important research priority.

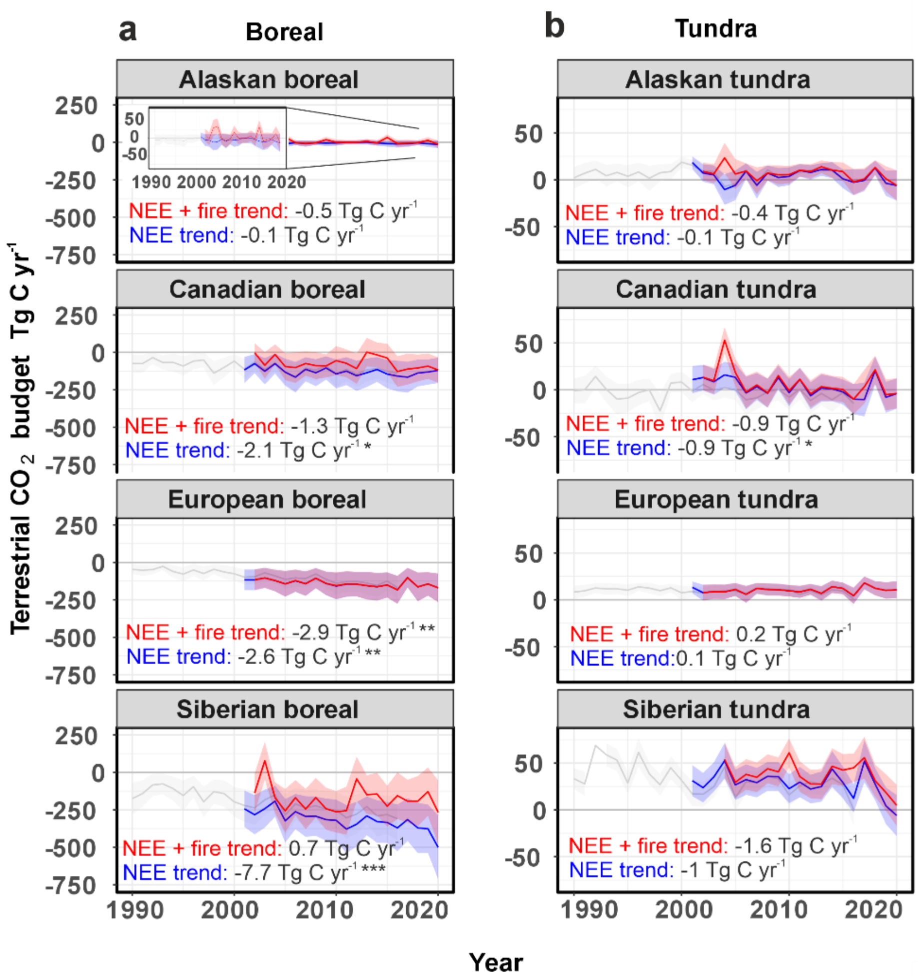

Figure 4. Terrestrial CO_2 budgets for NEE and NEE + fire in key regions and biomes across the boreal (a) and tundra (b). Terrestrial CO_2 budgets are shown for 1-km (blue; 2001-2020) and 8-km (grey; 1990-2016) NEE, and 1-km NEE + fire emissions (red; 2002-2020). Trends are shown for the 2002-2020 (NEE + fire) and 2001-2020 (NEE) periods. The inset in Alaskan boreal in (a) shows the time series with a narrower y axis compared to the main figure to better detect interannual variability. Uncertainties are standard deviations in bootstrapped estimates. Stars in the trend values depict the significance of the trend (= $p<0.05$, **=$p<0.01$, ***=$p<0.001$). Fire emissions alone are shown in Supplementary Fig. 16.*

Discussion

Our results show that the ABZ was on average an increasing terrestrial CO_2 sink (GPP is increasing more than R_{eco} + fire), indicating that the region still creates an important negative feedback to global warming. However, our study also suggests some positive feedbacks to climate change that have been more regional and of shorter duration in recent decades. We show that the presence of annual sources was large as indicated by several site-level and regional studies [35,36], and even larger with fire emissions included [37]. There were also extreme years when fire emissions exceeded annual net CO_2 uptake (e.g., 2003 in Siberian boreal, 2012 in Canadian boreal, and several years in the permafrost region; Fig. 2). Moreover, while summer net uptake increase still dominates over non-summer CO_2 emissions, net CO_2 uptake is increasing only in the early and peak growing season (May-August in the boreal and June-August in the tundra) and not in the late growing season (September), because GPP does not increase later in the season due to plant physiological limitations, and drier and warmer conditions cause enhanced R_{eco} instead [38–43]. A better understanding of how soil moisture and hydrology have been and will be changing, and the impact of these changes on CO_2 fluxes is critical for more accurate ABZ CO_2 budgets.

In the tundra, our findings reveal a noteworthy shift in carbon dynamics. While the tundra region has been a carbon sink for millennia [44], our results suggest that many tundra regions may now have started to function as CO_2 sources. This transition from an ecosystem CO_2 sink to a CO_2 source may have begun prior to 1990 [45], yet the precise timing of this transformation remains uncertain. The main drivers of this pattern may be related to warming-induced permafrost thaw, the drying of soils, or vegetation shifts [46–48] but remain unresolved. Tundra regions are also progressing towards conditions where average annual soil (0-7 cm) temperatures are above freezing, resulting in more soil organic material being susceptible to decomposition (Supplementary Fig. 12). Overall, the primary reason behind the annual CO_2 emissions from tundra ecosystems is the limited duration of the high net CO_2 uptake period, and the substantial non-summer season net emissions. However, we observed lower in-situ and upscaled October-April season NEE fluxes and budgets compared to Natali et al. (2019) throughout the entire period (Supplementary Fig. 19; [49]).

Our results demonstrate the need to further study Siberian CO_2 flux trends. Our upscaling indicated that some of the strongest net sources and sinks, and strongest increasing sink trends occur in the Siberian boreal. Increasing sink trends in Siberian tundra were also the strongest across tundra regions. The Siberian sink trend might be explained by strong greening trends [50], earlier growing season starts and increasing carbon uptake due to declining spring snow cover (Supplementary Fig. 14), increases in tree growth and distribution [51,52], rapid recovery of ecosystems after fire [53], and high cover of larch forests that can rapidly take up CO_2 (Supplementary Table 1)[8,54]. However, the large inversion model spread, sparse measurement network, and our upscaling uncertainties indicate that it remains challenging to conclude the magnitude of the Siberian CO_2 balance [2]. This is a significant problem given that Siberia stores more than half of the permafrost region's C stocks and is now warming more rapidly than other ABZ regions.

In summary, our study reveals distinct spatial and temporal patterns in CO_2 budgets across the ABZ and underscores the importance of three decades' worth of data. Relatively robust spatial patterns can be seen, such as the Alaskan CO_2 sources and southern Eurasian boreal sinks while the temporal trends remain more uncertain. While CO_2 fluxes can be relatively well modeled using machine learning and existing gridded datasets, gaps persist, such as the incomplete characterization of thermokarst and harvesting disturbances and their links to ecosystem CO_2 fluxes, and the lack of accurate predictors describing soil moisture [1]. Sustaining long-term sites is crucial to accurately track trends in ABZ CO_2 balance, while establishing new year-round sites in data-poor areas like Siberia and the Canadian Arctic is vital to fill knowledge gaps and enhance our understanding of carbon dynamics [55].

Online Methods

In-situ data overview

We used a recently compiled dataset of in-situ Arctic-boreal terrestrial ecosystem CO_2 flux measurements (ABCflux, led by Virkkala et al. 2021 [8]) within the ABZ (Supplementary Methods Section 1). The synthesized data were cumulative fluxes of gross NEE, GPP, and R_{eco} aggregated at the monthly timescale (3,968 to 4,897 site-months depending on the flux). In addition to eddy covariance data, we included fluxes estimated with the chamber method to increase data coverage especially during the growing season. The dataset included metadata out of which we used the site coordinate, biome, flux measurement method, and disturbance history information in the analysis. For further details on the dataset, see Virkkala et al. (2021) [8] and a description of additional data processing and screening in the Supplementary Methods Section 2. Note that our study does not include lateral transport of carbon which was recently summarized to be 93 Tg C yr^{-1} in a roughly similar region (i.e., 17 % of the net uptake budget calculated in this study) [56].

This dataset is more comprehensive than the ones used in earlier upscaling studies as it represents monthly fluxes from the entire year if available, while Virkkala et al. (2021) focused on coarse seasonal or annual fluxes [5], Natali et al. (2019) on monthly winter fluxes [9], and Mu et al. (2023) a more limited temporal period (2013-2017) [57]. Furthermore, we included more data from recent years (805 monthly observations from 2015-2020 compared to 32 and 95 fluxes in Virkkala et al. 2021 and Natali et al. 2019, respectively), and the sample size in our models was 4 to 25 times larger here compared to the earlier upscaling efforts.

Geospatial data

We used data from geospatial products as predictor variables to upscale fluxes. Our models had the following predictors: month, incident solar radiation, vapor pressure deficit, atmospheric CO_2 concentration, vegetation type, snow cover (the fraction covered by snow), soil temperature (0-7 cm), soil moisture (0-7 cm), NDVI (MODIS- or AVHRR-based), land surface temperature (or air temperature; MODIS- or ERA5 Land-based), compound topographic index (i.e., topographic wetness index), continuous vegetation fields describing percent non-tree vegetation and non-vegetated fraction and percent tree cover (MODIS- or AVHRR-based), soil pH (0-5 cm), soil organic carbon stock in 0-2 meters, and permafrost probability. In our analysis, NDVI was the primary predictor describing disturbances, with declines in NDVI being related to disturbances [5]. Data were in daily, weekly, monthly, annual, and static format (i.e., no temporal changes such as in the compound topographic index). If data were of higher temporal resolution than monthly, they were aggregated to monthly time steps. Gaps in MODIS and AVHRR NDVI time series were filled to produce a continuous time series. Data were re-projected to North Pole Lambert Azimuthal Equal Area Projection at 1 and 8 km spatial resolution and extracted at the flux sites. See Supplementary Section 3 for further descriptions and data sources.

We used the Global Fire Emissions Database (GFED) 500-m fire product [23] to calculate fire emissions. The product is based on a global fire emissions model with a spatial resolution of 500 m using MODIS data. The model was developed using an updated field measurement synthesis database of fuel load and consumption which included improvements, for example, in boreal soil carbon combustion. The higher resolution of the 500-m model compared to earlier coarser models improved the detection of small-scale fires and understanding of landscape heterogeneity, and reduced the scale mismatch in comparing field measurements to model grid cells. However, some small fires might still be undetected by this model, leading to potential underestimations in carbon emissions in this product.

Machine learning modeling

We used random forest models to upscale GPP, R_{eco}, and NEE to the ABZ from 1990 to 2020, the period with in-situ flux measurements. Two sets of predictive models were developed: (i) models using primarily predictors with a spatial resolution ≤1 km from 2001 to 2020 (i.e., the MODIS era) at 1-km spatial resolution (hereafter 1-km models;), and (ii) models using coarser-resolution predictors from the AVHRR GIMMS era (1990-2016;) from 1990 to 2016 at 8-km spatial resolution (hereafter 8-km models) (Supplementary Table 3). Each model included all available monthly fluxes from the entire year, i.e. no separate models for individual months or seasons were developed, as this approach resulted in the best predictive performance. All models included 17 predictors, but the sample sizes were variable depending on the amount of data available for each flux and time period; NEE models had the highest amount of model training data compared to GPP and R_{eco} models. For the 1-km model, coarsest predictors were at 9-km resolution but most important predictors were at 1 to 4-km resolution. For the 8-km model, the coarsest predictor resolution was 9 km, and the most important variables had a resolution of 1 to 9 km.

Model parameter tuning was performed based on leave-one-site out cross validation (CV) to achieve minimum predictive error. The models were run using the “caret” package in R version 4.2 [58]. We assessed the predictive performance of the final models using the (1) R^2, (2) root mean square error (RMSE), 3) mean absolute error (MAE), and 4) mean bias error (MBE) between predicted and observed values using the CV data. Larger RMSE and MAE values indicate larger errors, and positive MBE values indicate overestimation. The predictive performance of our models was good or high, ranging from 0.55 to 0.78 for R^2 and 19.4 to 37.3 g C m^{-2} $month^{-1}$ for RMSE, but was occasionally limited (Supplementary Fig. 1-3), mostly due to 1) our model not being able to identify landscape heterogeneity with nearby sites showing large differences in CO_2 fluxes (e.g., a forest and wetland site), and 2) our model not capturing inter-annual variability at individual sites, both of which are likely attributed to the coarse, uncertain, and missing predictors characterizing such conditions (e.g., soil moisture, disturbances).

We evaluated the uncertainty of predictions by creating 20 bootstrapped model training datasets (with replacement; same sample size as in the original model training data) and using those to develop 20 individual models and predictions. Out of the 20 predictions, we calculated the standard deviation to represent prediction uncertainty. The uncertainty ranges in NEE + fire budgets only represent NEE uncertainties. We further assessed the area of extrapolation of the models, and the influence of the flux measurement method and disturbance history information on flux predictions by training models with different subsets. Further details of the uncertainty analyses can be found in the Supplementary Methods Section 4.

Spatial upscaling of fluxes

We upscaled fluxes across the Arctic-boreal terrestrial area ≥49° N [59], which comprises 20.69 $\times 10^6$ km^2 of land (excluding glaciers and ice sheets; Fig. 1) with lake and glacier areas removed. The models were applied at a monthly time step from 2001 to 2020 for the 1-km models and from 1990 to 2016 for the 8-km models.

We analyzed the upscaled flux maps as well as environmental predictor rasters for temporal trends using the nonparametric Mann–Kendall test using the "zyp" package [60,61] with pre-whitening (Zhang method [62]) to remove autocorrelation. We report the significance of Kendall's correlation coefficient (the strength of the time-series) and the Theil–Sen slope to describe trends over time. Finally, we calculated zonal statistics of average annual, seasonal, and monthly fluxes and trends across key regions (Siberia defined as all land east from the Ural mountains, including a small portion of Mongolia; the rest of Eurasia, including Greenland are grouped within the European classes), biomes (tundra and boreal) [59], permafrost region [63], and vegetation types [8].

Comparison to process models and atmospheric inversions

We compared our estimates with the CMIP6 process models [26], atmospheric inversions used in the Global Carbon Project's Global Carbon Budget 2022 [64], and a global upscaling product FLUXCOM [25]. We included a subset of CMIP6 process models (13 in total) that had soil thermal processes at several depths to assure they had some information about the freeze-thaw patterns in the permafrost region. We included inversions with data from the whole 2001-2020 period (i.e., included five inversions and excluded four). Fire CO_2 emissions [23] were subtracted from the inversions. CMIP6 process model and FLUXCOM outputs were only available for the 2001-2014 and 2000-2013 period, respectively. The final model outputs used here represent terrestrial NEE (GPP-R_{eco}) in a similar way across the models except for inversions that also include vertical CO_2 fluxes from water bodies.

Acknowledgements

This work was supported by funding from the Gordon and Betty Moore Foundation (grant #8414) and funding catalyzed by the TED Audacious Project (Permafrost Pathways). We additionally acknowledge the funding from the NASA Arctic-Boreal Vulnerability Experiment and

Carbon Cycle Science programs (NNX17AE13G), NSF PLR Arctic System Science Research Networking Activities (RNA, Grant#1931333), Minderoo Foundation, KAKENHI(19H05668),The Danish National Research Foundation (CENPERM DNRF100), EU HORIZON GreenFeedBack, grant agreement No. 101056921, Danish Arctic Climate support through Greenland Ecosystem Monitoring and ICOS grants, Natural Sciences and Engineering Research Council, the Deutsche Forschungsgemeinschaft (DFG, German Research Foundation) under Germany's Excellence Strategy – EXC 2037 'CLICCS - Climate, Climatic Change, and Society' – Project Number: 390683824, NASA Grant/Cooperative Agreement Number: NNX17AD69A, The Research Council of Norway (BioGov, project nr. 323945), ERC synergy project Q-Arctic (grant agreement no. 951288), the Copernicus Atmosphere Monitoring Service, implemented by ECMWF on behalf of the European Commission (Grant: CAMS2 55), the Environment Research and Technology Development Fund of the Environmental Restoration and Conservation Agency of Japan (JPMEERF21S20810), ArCSII(JPMXD142031886), Financial support from the Swedish Research Council (VR) and consortium partners to ICOS Sweden (grants 2015−06020 and 2019−00205) and SITES (grant 2017−00635), VR grant 2019-04676 and 2018-03966, ArcticNet and NSERC,NOAA Cooperative Agreement NA16SEC4810008, Research Council of Finland (NPERM project nrs 341349, 330840, 349503 ICOS-FIRI), ICOS-FI via University of Helsinki funding, the EU Horizon Europe (GreenFeedback nr. 101056921 and LiweFor nr. 101079192), NRF-2021M1A5A1065425 (KOPRI-PN23011), NRF-2021M1A5A1065679, NRF-2021R1I1A1A01053870, the Dutch Research Council (NWO) (project number VI.Vidi.213.143), and The Natural Environment Research Council through the National Centre for Earth Observation (NE/R000115/1). Part of the research was carried out at the Jet Propulsion Laboratory, California Institute of Technology, under a contract with the National Aeronautics and Space Administration (80NM0018D0004). Part of the inverse analyses were performed on the supercomputer systems at the National Institute for Environmental Studies and Meteorological Research Institutes (NEC SX-Aurora TSUBASA and FUJITSU PRIMERGY CX2550M5) and at the HPC cluster Aether at the University of Bremen, financed by DFG within the scope of the Excellence Initiative (Germany).

Data availability

In-situ data used here can be accessed from ORNL DAAC [65]. Environmental predictors and links to the datasets are: TerraClimate (https://www.climatologylab.org/terraclimate.html), ERA5 Land (https://cds.climate.copernicus.eu/cdsapp#!/dataset/reanalysis-era5-land?tab=overview), MODIS land surface temperature MOD11A2v006 (https://lpdaac.usgs.gov/products/mod11a2v006/), Barrow CO_2 concentrations (doi:10.15138/yaf1-bk21), ESA CCI land cover (https://www.esa-landcover-cci.org/), CAVM vegetation type (https://geobotany.uaf.edu/), MODIS NDVI MOD13A1v006 (https://lpdaac.usgs.gov/products/mod13a1v006/), GIMMS3g NDVI (https://climatedataguide.ucar.edu/climate-data/ndvi-normalized-difference-vegetation-index-3rd-generation-nasagfsc-gimms), MOD44B continuous vegetation fields (https://developers.google.com/earth-engine/datasets/catalog/MODIS_006_MOD44B), MEaSUREs Vegetation Continuous Fields (https://lpdaac.usgs.gov/products/vcf5kyrv001/), ESA CCI permafrost probability (https://doi.pangaea.de/10.1594/PANGAEA.888600), SoilGrids (https://files.isric.org/soilgrids/former/2017-03-10/data/), MERIT DEM topographic indices (https://doi.pangaea.de/10.1594/PANGAEA.899135) (for more details see Supplementary Table 3). CMIP6 process model outputs can be accessed at https://aims2.llnl.gov/search/cmip6/, and Global Carbon Budget inversion outputs at https://meta.icos-cp.eu/objects/GahdRITjT22GGmq_GCi4o_wy (for more details see Supplementary Table 6). The 1-km and 8-km upscaled rasters of NEE, GPP, and R_{eco} together with their uncertainties will be published via ORNL DAAC upon publication.

Code availability

The main analysis codes can be found in the Supplement.

References

1. Watts, J. D. *et al.* Carbon uptake in Eurasian boreal forests dominates the high-latitude net ecosystem carbon budget. *Glob. Chang. Biol.* **29**, 1870–1889 (2023).
2. Fan, L. *et al.* Siberian carbon sink reduced by forest disturbances. *Nat. Geosci.* **16**, 56–62 (2022).
3. McGuire, A. D. *et al.* Dependence of the evolution of carbon dynamics in the northern permafrost region on the trajectory of climate change. *Proc. Natl. Acad. Sci. U. S. A.* **115**, 3882–3887 (2018).
4. McGuire, A. D. *et al.* Variability in the sensitivity among model simulations of permafrost and carbon dynamics in the permafrost region between 1960 and 2009. *Global Biogeochem. Cycles* **30**, 1015–1037 (2016).
5. Virkkala, A.-M. *et al.* Statistical upscaling of ecosystem CO2 fluxes across the terrestrial tundra and boreal domain: regional patterns and uncertainties. *Glob. Chang. Biol.* (2021) doi:10.1111/gcb.15659.
6. Pongracz, A., Wårlind, D., Miller, P. A. & Parmentier, F.-J. W. Model simulations of arctic biogeochemistry and permafrost extent are highly sensitive to the implemented snow scheme in LPJ-GUESS. *Biogeosciences* **18**, 5767–5787 (2021).
7. Pallandt, M. *et al.* Representativeness assessment of the pan-Arctic eddy-covariance site network, and optimized future enhancements. (2021) doi:10.5194/bg-2021-133.
8. Virkkala, A.-M. *et al.* The ABCflux database: Arctic-Boreal CO_2 flux observations and ancillary information aggregated to monthly time steps across terrestrial ecosystems. (2021) doi:10.5194/essd-2021-233.
9. Natali, S. M. *et al.* Large loss of CO2 in winter observed across the northern permafrost region. *Nat. Clim. Chang.* **9**, 852–857 (2019).
10. Hugelius, G. *et al.* Two decades of permafrost region CO2, CH4, and N2O budgets suggest

a small net greenhouse gas source to the atmosphere. *Authorea Preprints* (2023) doi:10.22541/essoar.169444320.01914726/v1.

11. Hugelius, G. *et al.* Estimated stocks of circumpolar permafrost carbon with quantified uncertainty ranges and identified data gaps. *Biogeosciences* **11**, (2014).
12. Schuur, E. A. G. *et al.* Permafrost and Climate Change: Carbon Cycle Feedbacks From the Warming Arctic. *Annu. Rev. Environ. Resour.* **47**, 343–371 (2022).
13. Rantanen, M. *et al.* The Arctic has warmed nearly four times faster than the globe since 1979. *Communications Earth & Environment* **3**, 1–10 (2022).
14. Berner, L. T. *et al.* Summer warming explains widespread but not uniform greening in the Arctic tundra biome. *Nat. Commun.* **11**, 4621 (2020).
15. Bjorkman, A. D. *et al.* Plant functional trait change across a warming tundra biome. *Nature* **562**, 57–62 (2018).
16. Lund, M. *et al.* Variability in exchange of CO2 across 12 northern peatland and tundra sites. *Glob. Chang. Biol.* **16**, 2436–2448 (2010).
17. Happonen, K., Virkkala, A.-M., Kemppinen, J., Niittynen, P. & Luoto, M. Relationships between above-ground plant traits and carbon cycling in tundra plant communities. *J. Ecol.* **110**, 700–716 (2022).
18. Euskirchen, E. S., Bret-Harte, M. S., Shaver, G. R., Edgar, C. W. & Romanovsky, V. E. Long-Term Release of Carbon Dioxide from Arctic Tundra Ecosystems in Alaska. *Ecosystems* **20**, 960–974 (2017).
19. Varner, R. K. *et al.* Permafrost thaw driven changes in hydrology and vegetation cover increase trace gas emissions and climate forcing in Stordalen Mire from 1970 to 2014. *Philos. Trans. A Math. Phys. Eng. Sci.* **380**, 20210022 (2022).
20. Arndt, K. A., Hashemi, J., Natali, S. M., Schiferl, L. D. & Virkkala, A.-M. Recent Advances and Challenges in Monitoring and Modeling Non-Growing Season Carbon Dioxide Fluxes from the Arctic Boreal Zone. *Current Climate Change Reports* **9**, 27–40 (2023).

21. Watts, J. D. et al. Regional hotspots of change in northern high latitudes informed by observations from space. *Authorea Preprints* (2024) doi:10.22541/au.170497370.03373595/v1. In review at Geophysical Research Letters.

22. See, C. R. et al. Decadal increases in carbon uptake offset by respiratory losses across northern permafrost ecosystems. In review at *Nature Climate Change* (2024).

23. van Wees, D. *et al.* Global biomass burning fuel consumption and emissions at 500 m spatial resolution based on the Global Fire Emissions Database (GFED). *Geosci. Model Dev.* **15**, 8411–8437 (2022).

24. Friedlingstein, P. *et al.* Global carbon budget 2021. *Earth Syst. Sci. Data* **14**, 1917–2005 (2022).

25. Jung, M. *et al.* Scaling carbon fluxes from eddy covariance sites to globe: synthesis and evaluation of the FLUXCOM approach. *Biogeosciences* **17**, 1343–1365 (2020).

26. Eyring, V. *et al.* Overview of the Coupled Model Intercomparison Project Phase 6 (CMIP6) experimental design and organization. *Geosci. Model Dev.* **9**, 1937–1958 (2016).

27. Ueyama, M. *et al.* Carbon dioxide balance in early-successional forests after forest fires in interior Alaska. *Agric. For. Meteorol.* **275**, 196–207 (2019).

28. Damgaard, C. A Critique of the Space-for-Time Substitution Practice in Community Ecology. *Trends Ecol. Evol.* **34**, 416–421 (2019).

29. Celis, G. *et al.* Tundra is a consistent source of CO2 at a site with progressive permafrost thaw during 6 years of chamber and eddy covariance measurements. *Journal of Geophysical Research: Biogeosciences* vol. 122 1471–1485 Preprint at https://doi.org/10.1002/2016jg003671 (2017).

30. Forkel, M. *et al.* Enhanced seasonal CO2 exchange caused by amplified plant productivity in northern ecosystems. *Science* **351**, 696–699 (2016).

31. Graven, H. D. *et al.* Enhanced seasonal exchange of CO2 by northern ecosystems since 1960. *Science* **341**, 1085–1089 (2013).

32. McGuire, A. D. *et al.* An assessment of the carbon balance of arctic tundra: comparisons among observations, process models, and atmospheric inversions. *Biogeosci. Discuss.* **9**, 4543 (2012).

33. Lin, X. *et al.* Siberian and temperate ecosystems shape Northern Hemisphere atmospheric CO2 seasonal amplification. *Proc. Natl. Acad. Sci. U. S. A.* **117**, 21079–21087 (2020).

34. Jorgenson, M. T., Racine, C. H., Walters, J. C. & Osterkamp, T. E. Permafrost Degradation and Ecological Changes Associated with a WarmingClimate in Central Alaska. *Clim. Change* **48**, 551–579 (2001).

35. Commane, R. *et al.* Carbon dioxide sources from Alaska driven by increasing early winter respiration from Arctic tundra. *Proc. Natl. Acad. Sci. U. S. A.* **114**, 5361–5366 (2017).

36. Euskirchen, E. S., Edgar, C. W., Turetsky, M. R., Waldrop, M. P. & Harden, J. W. Differential response of carbon fluxes to climate in three peatland ecosystems that vary in the presence and stability of permafrost. *J. Geophys. Res. Biogeosci.* **119**, 1576–1595 (2014).

37. Hayes, D. J. *et al.* Is the northern high-latitude land-based CO2sink weakening? *Global Biogeochemical Cycles* vol. 25 Preprint at https://doi.org/10.1029/2010gb003813 (2011).

38. Helbig, M. *et al.* Warming response of peatland CO2 sink is sensitive to seasonality in warming trends. *Nat. Clim. Chang.* **12**, 743–749 (2022).

39. Zona, D. *et al.* Pan-Arctic soil moisture control on tundra carbon sequestration and plant productivity. *Glob. Chang. Biol.* **29**, 1267–1281 (2023).

40. Zona, D. *et al.* Earlier snowmelt may lead to late season declines in plant productivity and carbon sequestration in Arctic tundra ecosystems. *Sci. Rep.* **12**, 3986 (2022).

41. Byrne, B. *et al.* Multi-year observations reveal a larger than expected autumn respiration signal across northeast Eurasia. *Biogeosciences* **19**, 4779–4799 (2022).

42. Pulliainen, J. *et al.* Early snowmelt significantly enhances boreal springtime carbon uptake. *Proc. Natl. Acad. Sci. U. S. A.* **114**, 11081–11086 (2017).

43. Parker, T. C., Unger, S. L., Moody, M. L., Tang, J. & Fetcher, N. Intraspecific variation in phenology offers resilience to climate change for Eriophorum vaginatum. *Arct. Sci.* 1–17 (2021).
44. Brovkin, V. *et al.* Comparative carbon cycle dynamics of the present and last interglacial. *Quat. Sci. Rev.* **137**, 15–32 (2016).
45. Oechel, W. C. *et al.* Recent change of Arctic tundra ecosystems from a net carbon dioxide sink to a source. *Nature* **361**, 520–523 (1993).
46. Lawrence, D. M., Koven, C. D., Swenson, S. C., Riley, W. J. & Slater, A. G. Permafrost thaw and resulting soil moisture changes regulate projected high-latitude CO2 and CH4 emissions. *Environ. Res. Lett.* **10**, 094011 (2015).
47. Parker, T. C., Subke, J.-A. & Wookey, P. A. Rapid carbon turnover beneath shrub and tree vegetation is associated with low soil carbon stocks at a subarctic treeline. *Glob. Chang. Biol.* **21**, 2070–2081 (2015).
48. Voigt, C. *et al.* Warming of subarctic tundra increases emissions of all three important greenhouse gases - carbon dioxide, methane, and nitrous oxide. *Glob. Chang. Biol.* **23**, 3121–3138 (2017).
49. Schiferl, L. D. *et al.* Using atmospheric observations to quantify annual biogenic carbon dioxide fluxes on the Alaska North Slope. *Biogeosciences* **19**, 5953–5972 (2022).
50. Piao, S. *et al.* Characteristics, drivers and feedbacks of global greening. *Nature Reviews Earth & Environment* **1**, 14–27 (2019).
51. Frost, G. V. & Epstein, H. E. Tall shrub and tree expansion in Siberian tundra ecotones since the 1960s. *Glob. Chang. Biol.* **20**, 1264–1277 (2014).
52. Kharuk, V. I., Ranson, K. J., Im, S. T. & Petrov, I. A. Climate-induced larch growth response within the central Siberian permafrost zone. *Environ. Res. Lett.* **10**, 125009 (2015).
53. Schulze, E.-D. *et al.* Factors promoting larch dominance in central Siberia: fire versus growth performance and implications for carbon dynamics at the boundary of evergreen

and deciduous conifers. *Biogeosciences* **9**, 1405–1421 (2012).

54. Hiyama, T. *et al.* Lessons learned from more than a decade of greenhouse gas flux measurements at boreal forests in eastern Siberia and interior Alaska. *Polar Sci.* **27**, 100607 (2021).
55. Pallandt, M. *et al.* High-latitude eddy covariance temporal network design and optimization. *Authorea Preprints* (2023) doi:10.22541/essoar.169755225.54015522/v1.
56. Ramage, J. L. *et al.* The net GHG balance and budget of the permafrost region (2000-2020) from ecosystem flux upscaling. *Authorea Preprints* (2023) doi:10.22541/essoar.169462008.85493456/v1.
57. Mu, C. *et al.* Ecosystem CO_2 exchange and its economic implications in northern permafrost regions in the 21st century. *Global Biogeochem. Cycles* **37**, (2023).
58. Kuhn, M. Building Predictive Models in R Using the caret Package. *J. Stat. Softw.* **28**, 1–26 (2008).
59. Dinerstein, E. *et al.* An Ecoregion-Based Approach to Protecting Half the Terrestrial Realm. *Bioscience* vol. 67 534–545 (2017).
60. Sen, P. K. Estimates of the Regression Coefficient Based on Kendall's Tau. *J. Am. Stat. Assoc.* **63**, 1379–1389 (1968).
61. Zhang + Yue-Pilon Trends Package [R package zyp version 0.11-1]. (2023).
62. Zhang, X., Vincent, L. A., Hogg, W. D. & Niitsoo, A. Temperature and precipitation trends in Canada during the 20th century. *Atmosphere-Ocean* **38**, 395–429 (2000).
63. Heginbottom, J., Brown, J., Ferrians, O. & Melnikov, E. S. Circum-arctic map of permafrost and ground-ice conditions, version 2. (2002) doi:10.7265/SKBG-KF16.
64. Friedlingstein, P. *et al.* Global carbon budget 2022. *Earth Syst. Sci. Data* **14**, 4811–4900 (2022).
65. Virkkala, A.-M. *et al.* The ABCflux Database: Arctic-boreal CO2 flux and site environmental data, 1989-2020. *ORNL DAAC* Preprint at https://doi.org/10.3334/ORNLDAAC/1934

(2021).